Author's personal copy

Optics Communications 284 (2011) 3785–3794

Contents lists available at ScienceDirect

Optics Communications

journal homepage: www.elsevier.com/locate/optcom

Single-shot multiple-delay crossed-beam spectral interferometry for measuring extremely complex pulses

Jacob Cohen [a], Pamela Bowlan [b], Vikrant Chauhan [a], Peter Vaughan [a], Rick Trebino [a,*]

[a] Georgia Institute of Technology, School of Physics, 837 State St, Atlanta, GA 30332, USA
[b] Max-Born-Institute, Max-Born Straße 2A, 12489 Berlin, Germany

ARTICLE INFO

Article history:
Received 15 December 2010
Received in revised form 26 February 2011
Accepted 27 February 2011
Available online 12 March 2011

Keywords:
Pulse measurement
Spectral interferometry
Complex pulses
Arbitrary waveforms

ABSTRACT

We demonstrate a single-shot measurement technique based on spectral interferometry (SI) for measuring the complete intensity and phase vs. time of extremely complex ultrashort laser pulses. Ordinarily, such a method would require an extremely-high-resolution spectrometer, but, by temporally interleaving many SI measurements, each using a different reference-pulse delay, our method overcomes this need. It involves introducing a transverse time delay into the reference pulse by tilting its pulse front transversely to the spectrometer dispersion plane. The tilted reference pulse then gates the unknown pulse by interfering with it at the image plane of a low-resolution imaging spectrometer, yielding an effective increase in the delay range and spectral resolution—by a factor of 30 in our proof-of-principle implementation. Our device achieved a temporal resolution of ~130 fs and a temporal range of 120 ps. This simple device has the potential to measure even longer and more complex pulses.

© 2011 Elsevier B.V. All rights reserved.

1. Complex ultrafast waveforms and their measurement

Recently there has been significant effort in the field of optical arbitrary-waveform generation [1], where a goal is to generate ~10 ns-long pulses with <100 fs structure. At the same time, this effort is also driving the field of optical metrology to develop new high-temporal- and high-spectral-resolution techniques [2–8] to measure such extremely complex waveforms.

The challenge in such measurements is attaining a large enough temporal range to measure the large temporal extent of the pulse, while simultaneously achieving a high temporal resolution to measure the fine temporal structure of the pulse. Alternatively, analogous spectral range and resolution conditions must be met if the measurement is performed in the frequency domain. Unfortunately, no measurement technique exists that can accomplish this—and to do so on a *single shot*, an additional requirement for measuring a true arbitrary waveform.

The measure of the complexity of a pulse is the time-bandwidth product, TBP $=\Delta t\ \Delta\nu$, where (in this work) Δt is the FWHM of the pulse temporal intensity and $\Delta\nu$ is the FHWM of the pulse spectrum. Using the above numbers, arbitrary-waveform generation can yield pulses with TBPs of ~100,000. For their measurement, commonly used self-referenced methods do not suffice, as they can characterize only very simple ultrashort pulses directly out of lasers. Of such methods, to our knowledge, only frequency-resolved optical gating (FROG) can measure pulses with time-bandwidth products greater than ~10. But self-referencing is unnecessary for most complex pulses, as complex pulses are usually generated from simpler pulses using an additional apparatus, so that an easily measurable reference pulse is available to assist in measuring the complex pulse.

When such a pre-characterized reference pulse is available, cross-correlation FROG (XFROG) has measured (continuum) pulses with TBPs up to 5000 [9]. Alternatively, sonogram methods [10–12]—mathematically equivalent to the spectrogram generated in XFROG [9]—are capable of similar-complexity measurements. But it would be difficult to extend these methods to pulses with much larger TBPs due to the very large data sets involved (N^2 points, where N is the length of the pulse field vector).

Additionally, several time-domain techniques based on temporal imaging can measure the temporal intensity of ps pulses [6,7] by stretching them to many ns in length, where detectors and oscilloscopes can accurately measure their intensities vs. time for potentially very complex pulses. In addition, high-bandwidth oscilloscopes and streak cameras can also measure the temporal intensity of longer, ps and ns, pulses. Heterodyning with a delayed version of the pulse or with another known pulse can yield the phase. Several techniques use this approach, including a variety of additional processes, such as four-wave-mixing in fibers [12]. However, these techniques involve a complex apparatus and/or expensive and fragile electronics.

In general, FROG and sonogram techniques have the great advantage that they involve two-dimensional data traces, which provide redundancy and internal corroboration of the measurement. But in the effort to measure extremely complex pulses, sacrifices must

* Corresponding author.
E-mail address: rick.trebino@physics.gatech.edu (R. Trebino).

0030-4018/$ – see front matter © 2011 Elsevier B.V. All rights reserved.
doi:10.1016/j.optcom.2011.02.078

Author's personal copy

be made, and this otherwise attractive feature is expendable. One technique that makes this sacrifice and has the potential to measure very complex waveforms is spectral interferometry (SI) [13]. In its simplest form, SI involves measuring the spectrum of the sum of two fields, that of a reference pulse and an unknown pulse. The result is a spectral interferogram from which both the amplitude and phase of the unknown pulse can be retrieved, provided that the reference pulse is known.

Although in principle SI is simple and high spectral resolution, in practice it is neither. Because it requires collinear pulses, it is very difficult to align and maintain aligned. And because it typically requires the reference pulse to be separated in time from the unknown pulse in order to make the spectral fringes required for pulse retrieval, its spectral resolution is limited to a factor of about five worse than that of the spectrometer used [14].

There have been numerous variations of SI, and some have improved its spectral resolution. For example, dual-quadrature SI (DQSI) [3,15], and even quadruple-quadrature SI (FQSI) [3], eliminate the pulse separation, but at a price of additional complexity and alignment sensitivity. Recently, Fontaine et al. demonstrated a "spectral interleaving" DQSI using multiple high-bandwidth oscilloscopes [3], which measure multiple spectral pieces of the pulse and concatenate them together. This technique offers a large temporal range: several microseconds. However, the temporal resolution is limited by that of the photo-detector and oscilloscope to about ~20 ps and so is inapplicable to ultrafast arbitrary waveform measurement. Alternatively, Asghari et al. demonstrated a time-domain variation of DQSI with 400 fs temporal resolution and 350 ps temporal range and used it to measure pulses with TBPs ~900. They achieved this by linearly chirping the pulse under test by a known (and large) amount, thereby mapping the individual spectral components of the pulse to time at an oscilloscope. Although this technique can be scaled to measure longer pulses with very fast update rates and high temporal resolution, it requires very accurate characterization of the dispersive medium in order to accurately map frequency to time.

It has also been proposed to significantly increase the finesse (and hence the measurable pulse complexity) of SI by using a variation of an echelle-type spectrometer that consists of a highly dispersive etalon with its dispersion orthogonal to that of the spectrometer diffraction grating [16], which yields a rectangular array that raster-scans the spectrum across the rectangular camera—a promising approach for measuring very complex pulses on a single shot. Its spectral resolution and accuracy are only limited by higher-order spectral variations of the dispersive elements, which could perhaps be compensated either optically or numerically.

Alternatively, it has been asserted that "time interleaving" [17] (measuring temporal pieces of the pulse separately and then concatenating them) could be the solution to the problem of measuring complex pulses on a single-shot. In previous work, we demonstrated a multi-shot time-interleaving technique that we call MUD TADPOLE. It has the ability to measure pulses with extremely large TBPs, and we have used it to measure pulses with TBPs of 65,000 [8]. MUD TADPOLE is a simple temporal scanning version of SEA TADPOLE [18–23], which is an experimentally simplified variation of SI that involves crossing *at an angle* the pulse to be measured with the previously measured reference pulse, which greatly simplifies alignment. The crossed beams generate a *spatial* interferogram [24,25]—unlike standard SI, which generates a *spectral* interferogram (the cause of the loss of spectral resolution), from which the unknown pulse's intensity and phase can be retrieved by *spatially* filtering the measured interferogram without loss of spectral resolution.

In this paper, we demonstrate a *single-shot* version of MUD TADPOLE, to our knowledge, the first single-shot technique for measuring complex waveforms that temporally interleaves many measurements with sub-ps temporal resolution and potentially nanosecond temporal range.

2. SEA TADPOLE and MUD TADPOLE

As mentioned, MUD TADPOLE shares a simple, yet powerful, feature with SEA TADPOLE and other crossed-beam SI methods: the required numerical filtering is accomplished using spatial fringes, rather than spectral fringes. Thus rather than separating the unknown and reference pulses in *time*, these methods separate them in *angle*. While SEA TADPOLE requires that the reference pulse at the output of the spectrometer (which expands inside the spectrometer to the reciprocal of its spectral resolution) be longer than the pulse to be measured, MUD TADPOLE does not make this assumption and instead takes advantage of the fact that the reference pulse generates spatial fringes *only* with the temporal piece of the unknown pulse with which it temporally overlaps. This allows multi-shot MUD TADPOLE to temporally scan the delay of the reference pulse, making numerous SEA TADPOLE measurements, something not possible in standard Fourier transform SI (FTSI), in which a large delay is required between the reference and unknown pulses.

We continue to exploit this advantage in single-shot MUD TADPOLE, making multiple SEA TADPOLE measurements at multiple delays—but on a single shot. We accomplish this by crossing the unknown pulse with a reference pulse with significant *pulse-front tilt* (PFT), generating a spatial interferogram similar to that obtained in SEA TADPOLE, except that now the delay varies spatially in the direction perpendicular to the spectral dispersion plane (see Fig. 1). Then a lens images the grating, mapping time to position at the camera.

Imaging the face of the grating onto the detector of the imaging spectrometer ensures that spatial dispersion (spatial chirp) is absent there and the main spatio-temporal distortion in the reference pulse is PFT (assuming the reference pulse was free of spatio-temporal distortions to begin with). This permits the use of a simple Fourier filtering technique [8] to retrieve the data.

The result is N SEA TADPOLE measurements of the electric field of the unknown pulse, each delayed in time by an amount proportional to the PFT, η (the time delay of the pulse front per unit transverse distance across the beam). Provided that the range of delays generated—the product of the PFT and the size of the camera at the output of the imaging spectrometer, Δx_c—is greater than or equal to the temporal length of the unknown pulse, τ_{unk}, or $\eta \cdot \Delta x_c \geq \tau_{unk}$, then the full temporal electric field of the unknown pulse can be

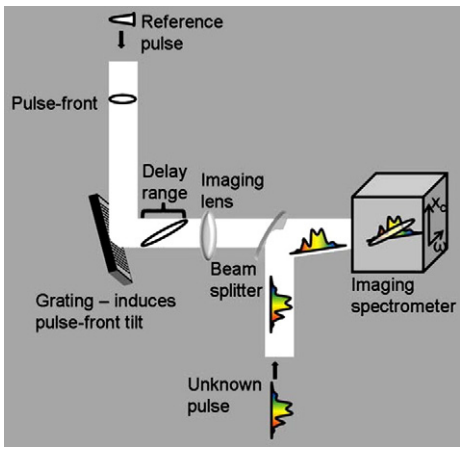

Fig. 1. Experimental setup for single-shot MUD TADPOLE. The pulse front of the spatially uniform reference pulse is tilted along the horizontal dimension by a grating. The imaging lens images the plane of the grating onto the detector of the imaging spectrometer, ensuring that spatial dispersion is absent and the main spatio-temporal coupling in the reference pulse is PFT. The unknown pulse is incident on the imaging spectrometer at a slight angle, θ, with respect to the reference pulse. This crossing of the two pulses results in a spatial interferogram with spatial fringes along the x_c dimension at the camera at the output of the imaging spectrometer.

Author's personal copy

reconstructed by temporally interleaving the N linearly delayed measurements.

Using PFT to increase the delay range to measure pulses has been well-documented in the literature [26,27]. Additionally, we recently used a crossed-beam SI method to measure the spatio-temporal field of a pulse with a PFT angle of ~89.9° and a delay range of several ns [28]. To our knowledge, however, there has been no use of PFT to temporally interleave measurements.

3. Single-shot MUD TADPOLE theory

The single-shot MUD TADPOLE retrieval algorithm consists of three steps, a spatial Fourier-filtering step, a temporal Fourier filtering step, and temporal concatenation. Although the single-shot MUD TADPOLE retrieval algorithm is very similar to that of multi-shot MUD TADPOLE [8] there are a few differences, and for that reason, we give a detailed explanation.

3.1. Step 1: Spatial Fourier filter

Single-shot MUD TADPOLE uses crossed-beam SI to generate the signal trace. In crossed-beam SI the electric field of the unknown pulse is retrieved from a spectrally resolved spatial interferogram resulting from the crossing of two beams. The interferogram is given by the following equation

$$S(\omega,x_c) = |E_u(\omega,x_c) + E_r(\omega,x_c)|^2, \tag{1}$$

where $E_u(\omega,x_c)$ and $E_r(\omega,x_c)$ are the electric fields of the unknown and reference pulse, respectively, and x_c is the spatial coordinate along the crossing dimension. The unknown beam is spatially uniform over the camera detector, and the electric field of the unknown pulse can be written in the form

$$E_u(\omega,x_c) = A_u(\omega-\omega_0)E_{u_x}(x_c)e^{i(\varphi_u(\omega-\omega_0))}, \tag{2}$$

where $A_u(\omega-\omega_0)$ and $\varphi_u(\omega-\omega_0)$ are the amplitude and phase of the unknown pulse, ω_0 is the center frequency, and $E_{u_x}(x_c)$ is the spatial dependence of the unknown pulse given by

$$E_{u_x}(x_c) = e^{i(kx_c\sin\theta)}, \tag{3}$$

where k is the wave-number and θ is the crossing angle of the unknown beam.

Similarly, we can model the spatio-temporal field of the reference pulse with PFT. To do so, we start in the (t, x_c) domain. In this domain the electric field of the reference pulse is given by

$$E_r(t,x_c) = E_{r_t}(t-\eta x_c)E_{r_x}(x_c), \tag{4}$$

where η is the PFT imparted by the grating. In Eq. (4) we have assumed that, apart from PFT, $E_r(t, x_c)$ has no additional spatio-temporal couplings of its coordinates. In other words, the reference pulse incident upon the diffraction grating must be spatially smooth with no spatio-temporal distortions. That both the reference and the unknown pulse must be spatially smooth with no spatial dependence is an important constraint for this technique, as with all other techniques that measure only the temporal behavior of the pulse.

Additionally in Eq. (4), the pulse-front tilt is given by $\eta=(\sin\theta_d+\sin\theta_i)/c=\lambda_0/(dc)$ in which θ_d is the diffracted angle from the grating, λ_0 is the center wavelength, θ_i is the incident angle on the grating, and d is the groove spacing of the grating. Taking a Fourier transform of Eq. (4) with respect to time yields

$$E_r(\omega,x_c) = E_{r_\omega}(\omega-\omega_0)E_{r_x}(x_c)e^{i\eta(\omega-\omega_0)x_c}. \tag{5}$$

Next, re-writing Eq. (5) in terms of the spectral amplitude and phase and crossing angle yields:

$$E_r(\omega,x_c) = A_r(\omega-\omega_0)e^{i(\varphi_r(\omega-\omega_0)-kx_c\sin\theta\ +\ \eta(\omega-\omega_0)x_c)}, \tag{6}$$

where $A_r(\omega-\omega_0)$ and $\varphi_r(\omega-\omega_0)$ are the spectral amplitude and phase of the reference pulse.

Substituting Eqs. (2) and (6) into Eq. (1) yields the intensity measured by the imaging spectrometer:

$$\begin{aligned} S(\omega,x_c) = {} & |A_u(\omega-\omega_0)|^2 + |A_r(\omega-\omega_0)|^2 \\ & + 2A_r(\omega-\omega_0)A_u(\omega-\omega_0)\cos[i(\Delta\varphi(\omega-\omega_0) \\ & + 2kx_c\theta + \eta(\omega-\omega_0)x_c)], \end{aligned} \tag{7}$$

where $\Delta\varphi(\omega-\omega_0)$ is the spectral phase difference between the reference and unknown pulse, c is the speed of light in vacuum, and we have used the small-angle approximation for the crossing angle, θ.

We use a Fourier retrieval algorithm [8] to filter the signal term from the interferogram. To do this we first take a spatial Fourier transform of Eqs. (7) and (8)

$$\begin{aligned} \tilde{S}(\omega,k_x) = {} & \left(|A_u(\omega-\omega_0)|^2 + |A_r(\omega-\omega_0)|^2\right)\delta(k_x) \\ & + \ldots 2A_r(\omega-\omega_0)A_u(\omega-\omega_0)e^{\pm i\Delta\varphi(\omega-\omega_0)} \\ & \times\delta\left(k_x \pm \left[2\frac{\omega}{c}\theta + \eta(\omega-\omega_0)\right]\right). \end{aligned} \tag{8}$$

Eq. (8) shows that the spatial Fourier transform has three terms. A DC background is located at $k_x=0$, and the signal term, which contains both the amplitude and phase of the unknown pulse, is off-center. The k_x-value of the signal term is determined by the crossing angle, θ, and the PFT, η, of the reference pulse.

In the filtering routine we isolate the signal term and shift it to the $k_x=0$ value, which is equivalent to adding a constant, $-2\omega_0\theta/c$, inside the delta function of the third term in Eq. (8). Therefore, after filtering and shifting, the retrieved signal term is

$$\begin{aligned} \tilde{S}_{retrieved}(\omega,k_x) = {} & A_r(\omega-\omega_0)A_u(\omega-\omega_0)e^{\pm i\Delta\varphi(\omega-\omega_0)} \\ & \times\delta\left(k_x \pm \left[\left(2\frac{\theta}{c} + \eta\right)(\omega-\omega_0)\right]\right). \end{aligned} \tag{9}$$

This term is then inverse Fourier transformed along the spatial domain, and the amplitude and phase of the reference pulse are divided out, yielding

$$\Psi(\omega,x_c) = A_u(\omega-\omega_0)e^{i\left[\varphi_u(\omega-\omega_0)\ +\ \left(2\frac{\theta}{c}\ +\ \eta\right)(\omega-\omega_0)x_c\right]}. \tag{10}$$

Eq. (10) is the retrieved field spectrogram shown in Fig. 2. By grouping different variables, we can rewrite Eq. (10) in a clearer fashion. First, we set

$$E(\omega-\omega_0) = A_u(\omega-\omega_0)e^{i\varphi_u(\omega-\omega_0)}. \tag{11}$$

This term is the electric field of the unknown pulse. Next, we set

$$\tau_x = (2\theta/c + \eta)x_c, \tag{12}$$

because the PFT maps position to delay. Substituting Eqs. (11) and (12) into Eq. (10) yields

$$\Psi(\omega,\tau_x) = E(\omega-\omega_0)e^{i(\omega-\omega_0)\tau_x}. \tag{13}$$

Author's personal copy

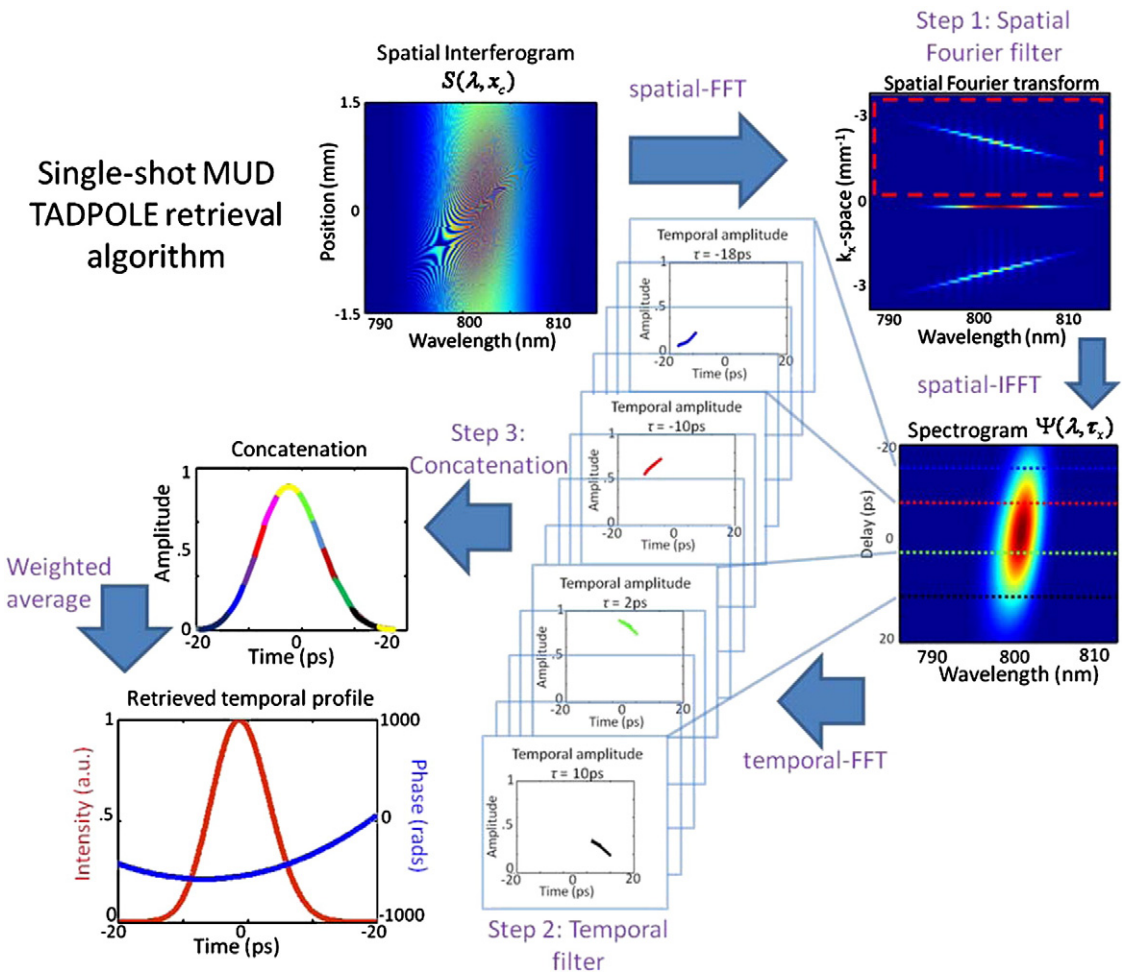

Fig. 2. The single-shot MUD TADPOLE retrieval algorithm of a chirped pulse. In Step 1, the MUD TADPOLE trace is spatially Fourier filtered. First the interferogram is spatially Fourier transformed along the x_c-axis. Then the signal term is filtered and shifted in k_x-space and inverse Fourier transformed back to the spatial domain. The amplitude and phase of the reference pulse are divided out of each row of the filtered image resulting in the field spectrogram (whose squared magnitude is the standard spectrogram). Each row of the complex spectrogram corresponds to the electric field of the unknown pulse at a different delay, $\Psi(\lambda,\tau_x)$. In Step 2, the retrieved fields are temporally filtered, keeping only the region in which the unknown and reference pulses are temporally overlapped. Each retrieved field, $\Psi(\lambda,\tau_x)$, is Fourier transformed to the time domain and temporally shifted to the lab frame yielding $\tilde{\Psi}_{lab}(t-\tau_x)$. In the figure, each color represents the retrieved field at a different delay. Although only the amplitudes are shown, the same process also yields the retrieved phases. In Step 3, the retrieved amplitude and phase are separately concatenated using a weighted average, resulting in the retrieved temporal profile of the entire unknown pulse.

Taking a 1-D Fourier transform of Eq. (13) along the spectral dimension yields

$$\tilde{\Psi}(t,\tau_x) = \tilde{E}\ \ (t+\tau_x)e^{i\omega_0 t}. \tag{14}$$

Eqs. (13) and (14) show that each row of the field spectrogram is the retrieved electric field, $\Psi(\omega,\tau_x)$, at a different delay, τ_x. Additionally Eq. (12) shows that τ_x varies linearly along the filtered spatial dimension of the imaging spectrometer. Therefore, a simple test pulse can be used to calibrate the delay axis, τ_x. For example, the experiments described in this paper used a double pulse of a known temporal separation for calibrating the delay axis.

3.2. Step 2: Temporal Fourier filter

Since Eq. (14) shows that the use of a reference pulse with PFT provides both (1) a range of delays and (2) *linearly* maps delay to position on the imaging spectrometer, we can reconstruct the entire unknown pulse in time by temporally interleaving the linearly delayed measurements in a similar fashion to the multi-shot MUD TADPOLE technique [8].

But before temporally interleaving, each delayed measurement must be temporally filtered because each section of the reference pulse only measures a small temporal range of the unknown pulse.

Temporal filtering is performed because each spatial section of the reference pulse interferes with a different temporal section of the unknown pulse of length τ_{sp} (see Fig. 3), which is smaller than the temporal length of the retrieved pulse, and only information within this region is kept, while that from larger and smaller times is discarded (see step 2 temporal filter in Fig. 2). The length of τ_{sp} is limited because each spectral measurement made by the detector only involves a temporal piece of the unknown pulse with a length up to the reciprocal of the spectral resolution of the spectrometer (the length of the reference pulse at the output of the spectrometer).

In this step, the spectrogram is first Fourier transformed along the spectral dimension to the time domain i.e.:

$$\Psi(\omega,\tau_x) \Rightarrow \tilde{\Psi}(t,\tau_x). \tag{15}$$

Next, we crop each field such that:

$$\tilde{\Psi}(t,\tau_x) = \begin{cases} \tilde{\Psi}(t,\tau_x) & \text{for } \tau_x - \frac{\tau_{sp}}{2} < t < \tau_x + \frac{\tau_{sp}}{2} \\ 0 & \text{otherwise} \end{cases}. \tag{16}$$

After temporally filtering, each retrieved electric field is shifted in time because each measurement is time averaged over the frame rate of the detector. In other words, the field retrieved at the delay τ_x on

Author's personal copy

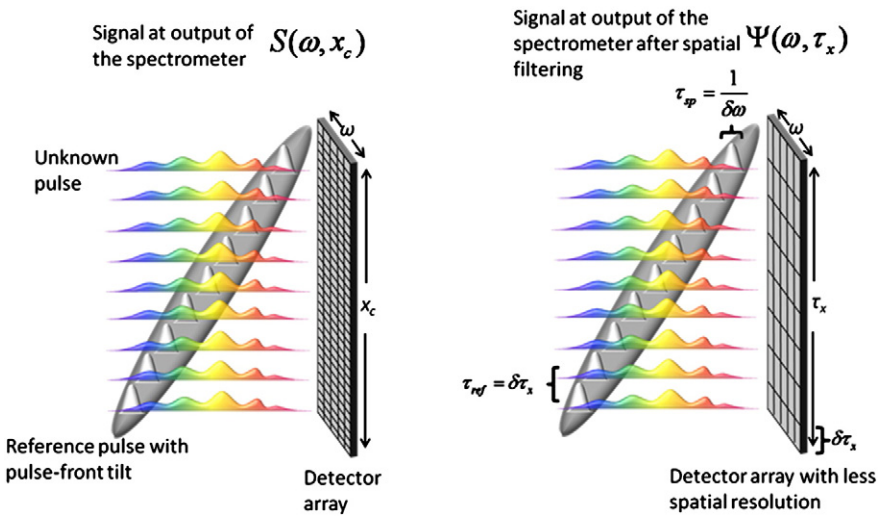

Fig. 3. The gating of the unknown pulse with the tilted reference pulse at the output of the spectrometer before and after spatial filtering. The spatial distribution of the unknown pulse is uniform over the entire detector, whereas the reference pulse exhibits PFT. The single-shot MUD TADPOLE trace, $S(\omega,x_c)$ is spatially filtered, yielding the field spectrogram, $\Psi(\omega,\tau_x)$. The spatial filtering effectively reduces the number of delayed spectral measurements. Additionally, due to the finite spectral resolution of the imaging spectrometer, each spectral measurement made by the detector measures only a section of the unknown pulse equal to the inverse of its spectral resolution, $\tau_{sp}=1/\delta\omega$.

the detector, $\tilde{\Psi}(t,\tau_x)$, is centered around $t=0$, the local zero time value of that measurement.

In order to concatenate the individual measurements, the retrieved fields must be transformed from the local time frame of each τ_x to the lab frame in which all of the spectral measurements occur at different times. This means that the retrieved field, $\tilde{\Psi}(t,\tau_x)$, is linearly shifted by τ_x,

$$\tilde{\Psi}(t,\tau_x) \Rightarrow \tilde{\Psi}_{lab}(t-\tau_x). \tag{17}$$

3.3. Step 3: Concatenation

After temporally filtering and shifting the retrieved fields to the lab frame, we can retrieve the full electric field of the unknown pulse by temporal interleaving or concatenating the sampled electric fields. To do this we use the concatenation and weighted averaging routine from Step 3 of the MUD TADPOLE retrieval algorithm detailed in [8].

In practice, we find it preferable to actually use delays, τ_{ref}, smaller than the length of the spectrometer-broadened reference pulse, τ_{sp}, in order to avoid using the weak leading and trailing regions of the product of the reference pulse and the retrieved temporal piece of the pulse.

Therefore a given section of the unknown pulse, $\tilde{\Psi}(t,\tau_x)$, is reliably retrieved by more than one reference pulse. We average together this redundant information to obtain a less noisy retrieved pulse. But due to the spectrometer's finite resolution, the accuracy of an individual measurement decreases for times further away from the reference pulse's temporal origin. The purpose of the weighting function is to account for this. Therefore, we choose the weighting function to be Gaussian (rather than square) so that it more heavily weighs information that originates from the temporal center of each measurement. Additionally, keeping the weighting function's width less than τ_{sp}, assures that no information from delays greater than τ_{sp}, is included in the average because this information is outside the spectrometer's temporal window and therefore not accurate. This process reduces the noise in the retrieved pulse and helps to avoid discontinuities when concatenating the independent measurements together.

Fig. 2 graphically represents the single-shot MUD TADPOLE retrieval algorithm.

4. Limitations on pulse-front-tilt, temporal range, and TBP

Although single-shot MUD TADPOLE has the unique property that it is not limited by the spectral resolution of the spectrometer, its spectral resolution cannot be increased without limit. Increasing the spectral resolution requires increasing the PFT of the reference pulse. Since PFT is a spatio-temporal coupling, a larger value will result in finer spatial fringes in the spatial interferogram. Finer spatial fringes will have a reduced contrast due to the limited spatial resolution of the imaging spectrometer. Therefore, both the crossing angle and the PFT that occur in the parameter τ_x in Eq. (12) must be chosen small enough so that the spatial resolution does not wash the fringes out entirely, and large enough so that the signal term can be extracted from the Fourier transform of the interferogram.

In this section we detail the limitations of single-shot MUD TADPOLE. First, we discuss how the PFT must be matched to the spectral and spatial resolution of the imaging spectrometer. Next, we derive the maximum PFT that can be used for single-shot MUD TADPOLE. Lastly, we derive the maximum TBP measurable.

4.1. Matching PFT to the spectral resolution of the spectrometer

The amount of PFT that can be used is determined by the limited *spectral* resolution of the imaging spectrometer. In single-shot MUD TADPOLE, an imaging spectrometer will make N measurements of the unknown pulse at N different delays. Fig. 3 illustrates the interference of the unknown pulse and the tilted reference pulse at the output of the imaging spectrometer.

Due to the spectrometer's finite spectral resolution, it measures a section of the unknown pulse up to the inverse of its spectral resolution, $\tau_{sp}=1/\delta\omega$. On the other hand, the temporal length of the reference pulse at a given delay is, τ_{ref}. Therefore, to ensure an accurate measurement of each section of the unknown pulse, the condition $\tau_{ref}<\tau_{sp}$ must be satisfied. If this condition is not met (because the PFT of the reference pulse is too large ($\tau_{ref}>\tau_{sp}$)) each spectral measurement will lack the appropriate spectral resolution to resolve those features of the unknown which are finer than the spectral resolution.

4.2. Matching the PFT to the spatial resolution of the imaging spectrometer

Not only must the PFT be matched to the spectral resolution, it must also be matched to the *spatial* resolution of the imaging

Author's personal copy

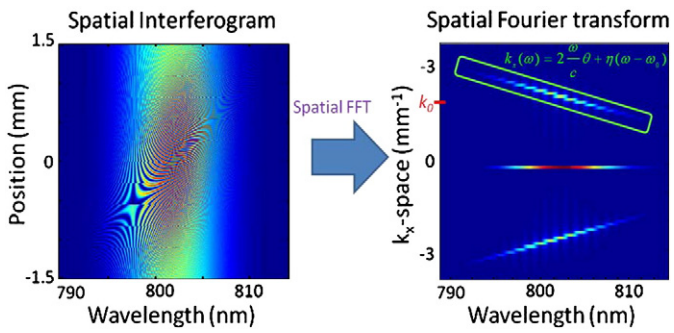

Fig. 4. The interferogram and the spatial Fourier transform of the interferogram. The green rectangle highlights the linear slope of the signal in k_x-space, and the equation governing the line is given by Eq. (17). Here k_0 is the center of the signal distribution in k_x-space.

spectrometer. In order to extract the signal term from the Fourier transform of the interferogram, it must be separated from the DC background in k_x-space. Eq. (7) shows the equation for the Fourier transform of the interferogram. The third term contains the signal and is therefore the term of interest. This term is a line in k_x-space (see Fig. 4) that is governed by the equation

$$k_x(\omega) = 2\frac{\omega}{c}\theta + \eta(\omega - \omega_0). \tag{18}$$

To avoid aliasing and to properly filter the signal term from the DC term, the condition $k_x > 0$ must be satisfied. Using this constraint and the fact that the above equation is smallest when $\omega = \omega_{min}$, we can solve for the maximum value of the PFT for a given crossing angle.

$$0 < 2\frac{\omega_{min}}{c}\theta + \eta(\omega_{min} - \omega_0). \tag{19}$$

Using the relation $\omega_{min} = \omega_0 - \Delta\omega/2$ and rearranging Eq. (19) to solve for the PFT

$$\eta < \frac{4\theta(\omega_0 - \Delta\omega/2)}{\Delta\omega c}. \tag{20}$$

For the maximum PFT, the inequality in Eqs. (20) and (21) becomes an equality.

To allow for the maximum value of PFT, the center of the signal distribution given by Eq. (20) will be located in the center of the upper half of the Fourier transformed image shown in Fig. 4 or

$$k_0 = \frac{\pi}{2\delta x_c}, \tag{21}$$

where, δx_c is the pixel width. Using Eqs. (18) and (21) we can solve for the crossing angle of the center frequency

$$\theta_0 = \frac{c\pi}{4\delta x \omega_0}. \tag{22}$$

Using $\lambda_0 = 800$ nm and a pixel width of 3.5 μm, $\delta x = 3.5$ μm, Eq. (22) yields a crossing angle of ~1°.

Using Eqs. (20) and (22), we can solve for the maximum amount of PFT that can be used to measure a pulse with single-shot MUD TADPOLE.

$$\eta_{\max} = \frac{\pi}{\delta x_c \omega_0}\left(\frac{\omega_0}{\Delta\omega} - \frac{1}{2}\right). \tag{23}$$

A spectral range of ~20 nm, a center wavelength of ~800 nm, and a pixel size of 3.5 μm, yield a value for the maximum possible PFT: $\eta_{\max} = 0.015$ fs/nm.

The temporal range is given by the product of the PFT and the spatial extent of the imaging spectrometer

$$\Delta t = \eta \cdot \Delta x_c = \eta \cdot N_x \cdot \delta x_c. \tag{24}$$

where N_x is the number of points along the spatial dimension of the imaging spectrometer.

Using Eqs. (23) and (24) the maximum temporal range can be calculated

$$\Delta t = \frac{\pi N_x}{\omega_0}\left(\frac{\omega_0}{\Delta\omega} - \frac{1}{2}\right). \tag{25}$$

For the experimental parameters used in this paper, a spectral range of ~20 nm, center wavelength of ~800 nm, a pixel size of 3.5 μm, and a camera with 3000 pixels in the spatial dimension yield a maximum temporal range of $\Delta t = 158$ ps.

4.3. TBP limitations

Now that we have found the maximum PFT, we can solve for the maximum TBP measurable by single-shot MUD TADPOLE. Using Eq. (25) the maximum TBP is

$$\mathrm{TBP} = \Delta t \Delta f = \frac{N_x \pi}{2}\left(1 - \frac{\Delta\omega}{2\omega_0}\right). \tag{26}$$

Using the experimental parameters used in this paper, the maximum TBP is ~4500. It is worth noting that the maximum TBP that MUD TADPOLE can measure is proportional to the number of pixels along the spatial dimension. Therefore, if we were to use a custom, rectangular 6-megapixel detector array (30,000 × 200), and keep the spectral range constant, then the maximum TBP would be 45,000, which corresponds to a 20 nm pulse centered at 800 nm that has been stretched to ~5 ns in length.

5. Experimental setup

We performed experiments using a Coherent MIRA Ti:Sapphire oscillator. The pulses were centered at 809 nm, with a FWHM bandwidth of 7.9 nm (3.7 THz), at a repetition rate of 76 MHz, and had pulse energies of ~5.2 nJ per pulse. Using a Swamp Optics GRENOUILLE 8-50USB [9], the input pulse was measured to have a temporal width of 130 fs (see Fig. 5).

A simplified version of the single-shot MUD TADPOLE experimental set-up is illustrated in Fig. 1. The reference pulse is incident upon a 10.5 cm × 10.5 cm 1200 grooves/mm grating at near grazing incidence, ~89° with respect to the grating normal. The near-grazing incidence caused the reference beam to fill the entire 10.5 cm grating, which maximized the amount of PFT induced along the horizontal dimension.

The pulse at the surface of the grating was imaged by a two-lens imaging system that also de-magnified the beam by a factor 2.5. The reason for de-magnifying the beam was to increase the PFT of the reference pulse, thereby increasing the range of delay by a factor equal to the de-magnification, 2.5. The two-lens imaging system imaged the plane of the grating onto the detector of the imaging spectrometer, which ensured that the main spatio-temporal coupling in the reference pulse was PFT and that spatial chirp was absent.

A periscope was used to rotate the reference pulse out of the plane such that the PFT occurred in the vertical dimension. This was done because the imaging spectrometer spectrally resolved the beam along the horizontal dimension.

Author's personal copy

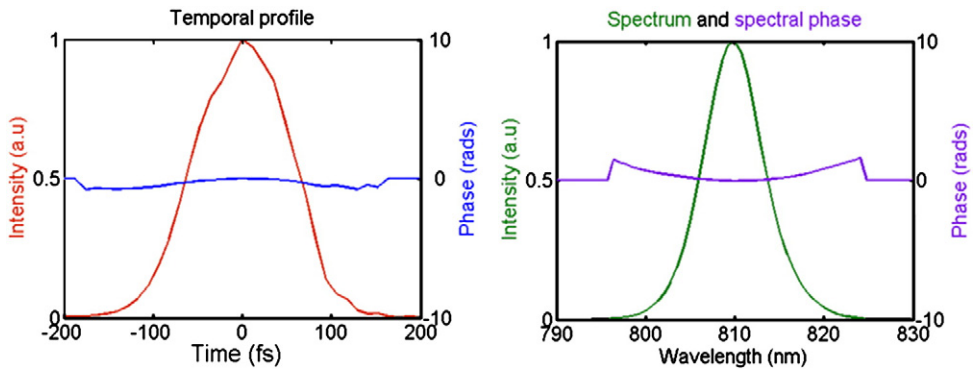

Fig. 5. The temporal and spectral profiles of the input pulse used in the experiments. The FHWM bandwidth of the input pulse was 7.9 nm and the FWHM temporal width was 130 fs. The measured input pulse was close to transform limited as evidenced by the slight quadratic spectral phase displayed in the spectral plot.

The imaging spectrometer consisted of a 600 groove/mm grating and a 100 cm focal length cylindrical lens. A CMOS detector with 3000×2208 pixels collected the image. The imaging spectrometer used in this setup had a spectral resolution of $\delta\lambda = 0.04$ nm/pixel. We measured the temporal response function (see Fig. 6(a)) of the spectrometer by measuring the spectral fringe contrast due to two temporally overlapped pulses at varying delays [8,14].

Due to the relatively slow shutter speed of our camera (~ms), and the relatively high repetition rate of our laser, 76 MHz, we could not make a true single-shot measurement. Instead all measurements described in this paper reflect instead *single-frame* measurements, or measurements made using one camera frame, rather than one laser pulse. Regardless, the technique described in the paper could easily be performed on a single shot if a fast enough camera is available or a low enough repetition rate pulse train were used.

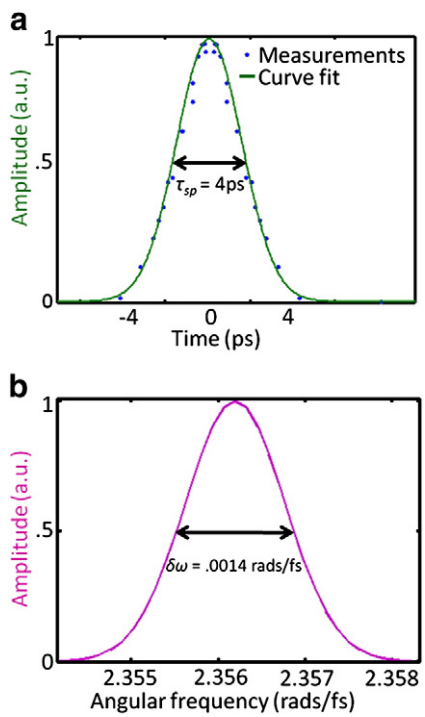

Fig. 6. a. The temporal response function, $h(t)$, of the imaging spectrometer used in the experiments in this paper. We measured the response function (dots) using a Michelson interferometer, which generated a double pulse with variable pulse separation. The solid curve is a fit to the data. b. The Fourier transform of $h(t)$, which is the spectral response function, $H(\omega)$. Note that we only measured $h(t)$ on one side of the time axis because we expect it to be a symmetric function because $H(\omega)$ is a real function. The measured FWHM of the temporal response function, τ_{sp}, was 4 ps. Therefore, the imaging spectrometer can only accurately measure the spectrum of pulses with lengths < 4 ps, or equivalently, pulses with spectral features $\delta\omega > 0.0014$ rads/fs.

The FWHM of the temporal response function was experimentally determined to be $\tau_{sp} = 4$ ps.

Additionally, the temporal resolution of single-shot MUD TADPOLE is determined from the spectral range, which in this experiment was 17 nm, resulting in a temporal resolution of 130 fs.

Finally, to ensure that the unknown pulse was spatially uniform over the spatial range of the imaging spectrometer, a short 35 cm fiber was used as the input of the unknown pulse. A 150 mm focal length lens located a focal length away from the output of the fiber was used to collimate the output incident upon the imaging spectrometer.

6. Results and discussion

We performed two experiments to demonstrate single-shot MUD TADPOLE's large temporal range/high spectral resolution. These experiments demonstrate how single-shot MUD TADPOLE dramatically improves the spectral resolution of the imaging spectrometer. In both experiments single-shot MUD TADPOLE provides the necessary spectral resolution to completely characterize the intensity and phase of the unknown pulse.

Fig. 7 shows the single-shot MUD TADPOLE measurement of a train of four pulses separated by ~7 ps. The train of pulses was generated using an etalon composed of two partially reflecting mirrors with a reflectivity of 90%.

Fig. 7(a) shows the single-shot MUD TADPOLE trace. The spatial fringes (the signal term) generated from the interference between the unknown and the reference pulses are almost entirely washed out. This is because, on each row of the detector, the reference pulse only makes spatial fringes with the temporal piece of the unknown pulse with which it temporally overlaps. The rest of the unknown pulse also inevitably impinges on the camera (see Fig. 3), yielding a spatially structureless background of no value to that particular measurement and which must therefore be filtered out. This background is filtered out by performing a spatial Fourier transform (see Fig. 7(b)). The image of the Fourier transform of the trace clearly shows the signal term.

After the signal term is filtered and shifted in k_x-space, it is inverse Fourier transformed back to the spatial domain, and the amplitude of the reference pulse is divided out.

Additionally, the spectral phase of the reference pulse is subtracted out, resulting in the spectral phase of the unknown pulse, as described in Section 3.1, Eqs. (9) and (10). Since the reference pulse was derived directly from the input pulse, their spectral phase and amplitude were identical with the exception of the linear pulse-front-tilt term of the reference pulse displayed in Eq. (6). However, since only spectral

Author's personal copy

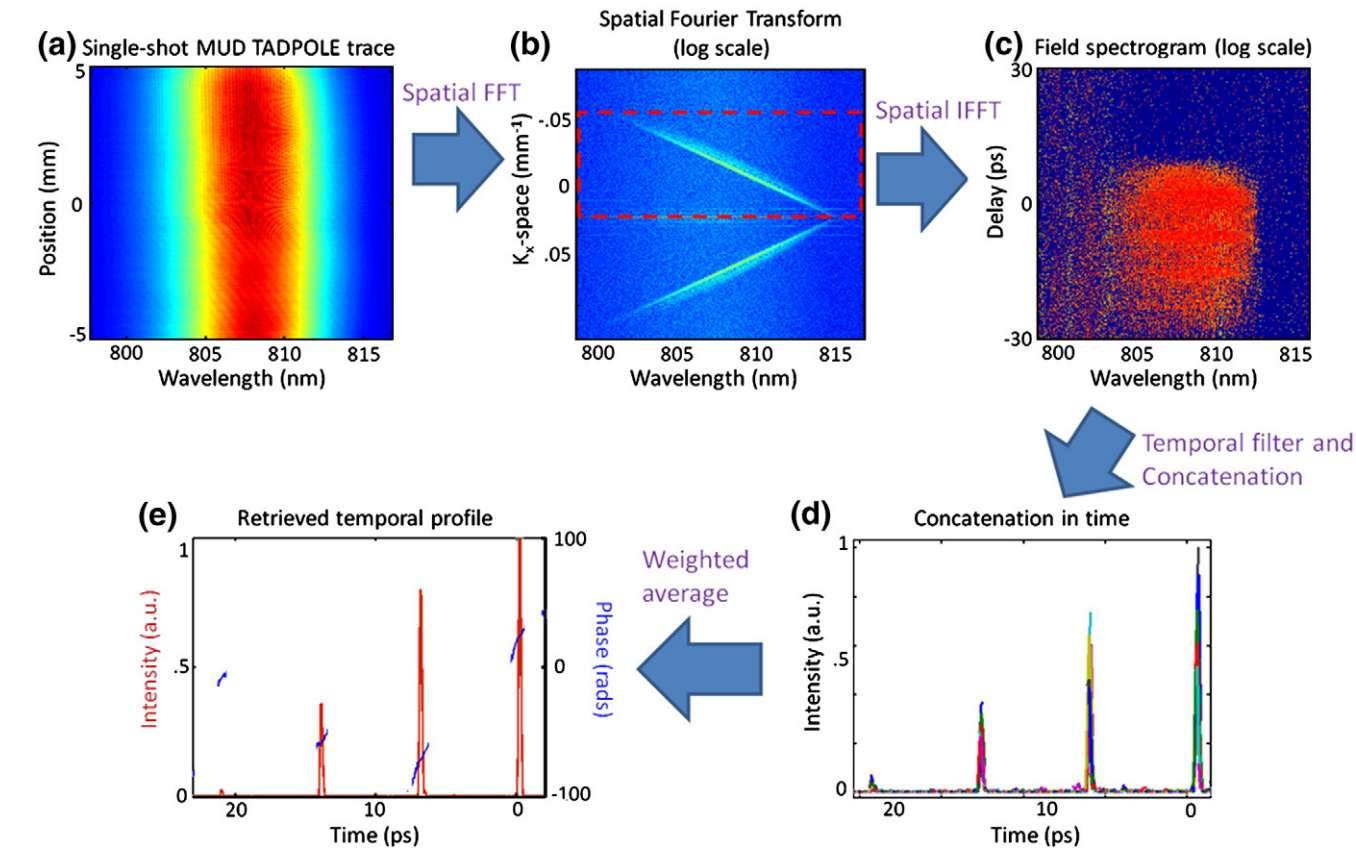

Fig. 7. Single-shot MUD TADPOLE measurement of a 21 ps pulse train. a. The single-shot MUD TADPOLE trace. b. The spatial Fourier transform of the trace. Here the signal term is filtered in k_x-space and inverse Fourier transformed back to the spatial domain. c. The field spectrogram, where we have transformed the spatial axis to the delay axis because of the PFT of the reference pulse. d. The concatenation step of the MUD TADPOLE retrieval algorithm in which the retrieved sections of the unknown pulse are concatenated in time. Here each color represents the retrieved temporal intensity at a different delay. e. After performing a weighted average over all the retrieved sections of the unknown pulse's amplitude and phase, the full temporal electric field of the unknown pulse is retrieved.

phase terms 2nd order and higher are relevant to the characterization of a pulse, subtracting off the measured spectral phase of the input pulse (see Fig. 5) completely determined the spectral phase of the unknown pulse.

The field spectrogram is shown in Fig. 7(c). Here we have transformed the spatial dimension to delay, because the PFT of the reference pulse linearly maps position to delay on the camera. The calibration of the delay axis was determined using a double pulse of a known temporal spacing.

Next, the spectrogram is Fourier transformed along the spectral dimension to the "time" domain, and temporally filtered keeping only the region in which the unknown and the section of the reference pulse that temporally overlap. Fig. 7(d) shows how the delayed sections of the unknown pulse are then concatenated in time. Using the weighted averaging scheme described in [8], the delayed retrieved sections of the pulse are averaged together, resulting in the full temporal profile of the unknown pulse (see Fig. 7(e)).

Fig. 7(e) shows that the pulse train had a length of ~21 ps, which is ~5 times larger than the FWHM of the temporal response function, τ_{sp}, of the spectrometer used (see Fig. 6(a)). Accordingly, the single-shot MUD TADPOLE technique increased the temporal range/spectral resolution of the imaging spectrometer by a factor of 5. Therefore, had we not used the single-shot MUD TADPOLE technique, the imaging spectrometer would only be capable of accurately measuring one of the four pulses in the pulse train.

We compared the retrieved spectrum to that of an Ocean Optics HR 4000 spectrometer shown in Fig. 8. Comparing the MUD TADPOLE retrieved spectrum to that of a commercial spectrometer is a good way to test the accuracy of the single-shot MUD TADPOLE technique. The good agreement between the two independently measured spectra confirms that the temporal profile measured in Fig. 7(e) is that of the unknown pulse.

Our next experiment highlighted the high temporal resolution of MUD TADPOLE. In this experiment we measured a chirped double pulse at multiple delays.

The double pulse was generated by a Michelson interferometer. After the Michelson interferometer, we chirped the pulses with a single-grating pulse compressor [8].

Fig. 9 shows both the measured and simulated temporal intensity and phase of two linearly chirped pulses at variable delays with

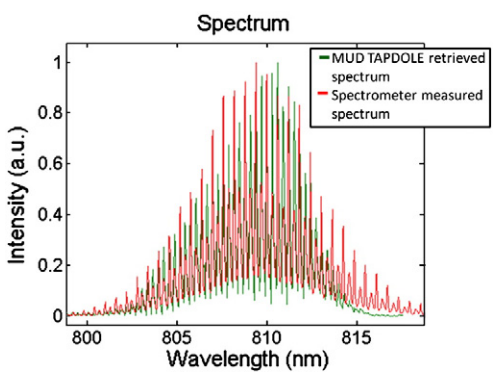

Fig. 8. A comparison of the MUD TADPOLE retrieved spectrum and a spectrometer measured spectrum. The agreement between the two spectra confirms the accuracy of the MUD TADPOLE measurement shown in Fig. 7.

Author's personal copy

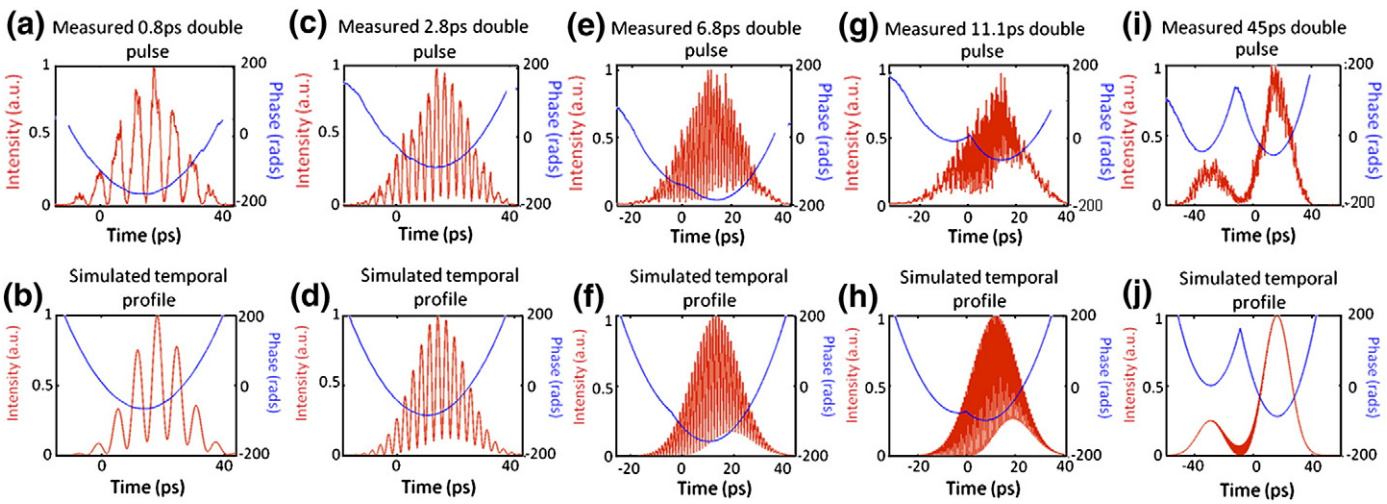

Fig. 9. A comparison of the measured and calculated temporal profiles of a chirped double pulse at variable delays. a,b. The MUD TADPOLE retrieved and simulated temporal profiles of two 21 ps linearly chirped pulses separated by 0.8 ps. c,d. The retrieved and simulated temporal profiles after increasing the delay between pulses to 2.8 ps. e,f. The retrieved and simulated temporal profiles after increasing the delay between pulses to 6.8 ps. At this large delay the temporal phase develops a cusp, which MUD TADPOLE is able to retrieve. g,h. The retrieved and simulated temporal profiles after increasing the delay between pulses to 11.1 ps. i,j. The retrieved and simulated temporal profiles after increasing the delay between pulses to 45 ps. In this measurement the pulses are separated by a large delay, yet there is still some temporal overlap. This results in very high frequency temporal beating. In all measurements, the agreement between the expected and measured results is good.

respect to one another. Fig. 9 demonstrates a phenomenon known as chirped pulse beating [29], which occurs because, at each point in time, the frequency content of each pulse differs by a constant beat frequency. This beat frequency is proportional to the delay, τ, between the two pulses.

Fig. 9 simultaneously highlights the high temporal resolution and the large temporal range of MUD TADPOLE. The temporal resolution of MUD TADPOLE is determined by the spectral range of the spectrometer used in Fig. 1. In this experiment, our spectrometer had a spectral range of 17 nm and a temporal resolution of 130 fs. This high temporal resolution was put to good use in the measurement of the double pulse with an 11 ps delay shown in Fig. 9(g). The fast temporal beating, which had a temporal period of 510 fs, is well resolved by MUD TADPOLE.

In addition to accurately measuring very fine temporal intensity features, MUD TADPOLE can also measure complicated temporal phases. This is demonstrated in Fig. 9(e, g, and h), which shows the development of a phase cusp, which becomes more prevalent as the delay between the two linearly chirped pulses is increased.

7. Summary and limitations

We have introduced the first single-shot ultrashort pulse measurement technique that temporally interleaves hundreds of measurements for the complete measurement of the electric field of relatively long pulses (>100 ps) with ~fs temporal resolution. The experiments described above resulted in an increase in the spectral resolution of the spectrometer used by a factor of 30 (120 ps/4 ps). Furthermore, we have used it to measure pulses up to ~80 ps (see Fig. 9) with TBPs up to 296 (80 ps × 3.7 THz).

Although the demonstrated temporal range was ~120 ps, the temporal range/spectral resolution of single-shot MUD TADPOLE can be increased by either increasing the pulse front-tilt or using a larger detector array. The PFT can be increased by using a grating or etalon with larger PFT or de-magnifying the image of the reference pulse on the grating by a larger amount.

It must be noted that increasing the PFT (or equivalently the angular dispersion) to too large a value will make the equation for PFT nonlinear (see Eqs. (3) and (4)). The result of this is that the transverse time delay of the reference pulse front will be nonlinear, and the delay between individual spectral measurements will not be constant. This effect can be calibrated using a simple test pulse.

Furthermore, there are a number of experimental constraints on both the reference and unknown pulses. First, apart from the pulse-front tilt of the reference pulse, both the reference pulse and the unknown pulse must be both spatially uniform and have no spatio-temporal distortions. The reason for this is that position is mapped to delay on the imaging spectrometer and a spatial distortion in either of the beams will distort the resulting measurement. For this reason, we recommend using an input fiber or pinhole to spatially filter the unknown beam before the imaging spectrometer. Additionally, like all other versions of SI, the reference pulse must be well-characterized and it must contain all the frequencies of the unknown pulse in order for interference to occur.

Additionally, the temporal range and hence complexity of pulse that can be measured cannot be increased without limit due to the finite spatial resolution of the imaging spectrometer and dynamic range of the camera.

Finally, the dynamic range of the camera is also limiting factor. For extremely long pulses, the fringes due to the temporal overlap with the reference pulse will be obscured by potentially more intense DC terms due to the rest of the complex unknown pulse that does not temporally overlap with the reference pulse. In other words, as the unknown pulse duration increases, the fringe contrast will decrease because fringes only occur when the pulses temporally overlap, so most of the intensity will be in this DC background. If, for example, the unknown pulse has a temporal length of τ_{sp}, then only one measurement is required (and MUD TADPOLE reduces to SEA TADPOLE), and the ratio between the signal term (spatial fringes) and the DC term (background) will be 1/2 (assuming the intensities of the two pulses are equal). If the unknown pulse has a temporal length of $2\tau_{sp}$, then one extra reference pulse will be required, and one extra signal term will be added, and the ratio becomes 1/3. If the unknown pulse has a temporal length of $3\tau_{sp}$, the ratio becomes 1/4, etc. Therefore, for a MUD TADPOLE setup that measures a pulse with a length of $N\tau_{sp}$, the ratio of the signal to background will be $1/(N+1)$. Thus, a 10 bit camera with 1024 counts could be used to measure a pulse requiring no more than 1023 individual measurements, yielding at most a factor of 1023 improved spectral resolution.

Nevertheless, for a single-shot MUD TADPOLE using a few-megapixel camera and a low resolution spectrometer with 20 nm

Author's personal copy

spectral range, the maximum TBP that can be measured is ~4500. Therefore, we believe that this simple and inexpensive device can be used to accurately characterize stretched pulses used in CPA systems and provide the foundation for the measurement of arbitrary waveforms. Furthermore, even if the spectral phase is not desired, it could be used simply to improve the spectral resolution of any spectrometer.

Acknowledgments

This study was supported by the Georgia Institute of Technology TI:GER program and the Georgia Research Alliance.

References

[1] J. Zhi, H. Chen-Bin, D.E. Leaird, A.M. Weiner, Nat. Photonics 1 (2007) 463.
[2] V.R. Supradeepa, C.M. Long, D.E. Leaird, A.M. Weiner, Opt. Express 18 (2010) 18171.
[3] N.K. Fontaine, R.P. Scott, L. Zhou, F.M. Soares, J.P. Heritage, and S.J.B. Yoo, Nat. Photonics, 4 248.
[4] M.H. Asghari, Y. Park, J. Azaña, Opt. Express 18 (2010) 16526.
[5] V.R. Supradeepa, D.E. Leaird, A.M. Weiner, Opt. Express 17 (2009) 14433.
[6] M.A. Foster, S. Salem, D.F. Geraghty, A. Turner-Foster, M. Lipson, A.L. Gaeta, Nature 456 (2008) 81.
[7] D.H. Broaddus, M.A. Foster, O. Kuzucu, A.C. Turner-Foster, K.W. Koch, M. Lipson, A.L. Gaeta, Opt. Express 18 (2010) 14262.
[8] J. Cohen, P. Bowlan, V. Chauhan, R. Trebino, Opt. Express 18 (2010) 6583.
[9] X. Gu, L. Xu, M. Kimmel, E. Zeek, P. O'Shea, A.P. Shreenath, R. Trebino, R.S. Windeler, Opt. Lett. 27 (2002) 1174.
[10] M. Vampouille, A. Barthélémy, B. Colombeau, C. Froely, J. Opt. (Paris) 15 (1984) 385.
[11] E.J.R. Kelleher, J.C. Travers, E.P. Ippen, Z. Sun, A.C. Ferrari, S.V. Popov, J.R. Taylor, Opt. Lett. 34 (2009) 3526.
[12] M. Skold, M. Westlund, H. Sunnerud, P.A. Andrekson, J. Lightwave Technol. 27 (2009) 3662.
[13] C. Froehly, A. Lacourt, J.C. Vienot, Nouv. Rev. Opt. 4 (1973) 183.
[14] C. Dorrer, N. Belabas, J.-P. Likforman, M. Joffre, J. Opt. Soc. Am. B 17 (2000) 1795.
[15] L. Lepetit, G. Cheriaux, M. Joffre, J. Opt. Soc. Am. B 12 (1995) 2467.
[16] S.A. Diddams, L. Hollberg, V. Mbele, Nature 445 (2007) 627.
[17] Y. Han, B. Jalali, J. Lightwave Technol. 21 (2003) 3085.
[18] P. Bowlan, U. Fuchs, R. Trebino, U.D. Zeitner, Opt. Express 16 (2008) 13663.
[19] P. Bowlan, P. Gabolde, M.A. Coughlan, R. Trebino, R.J. Levis, J. Opt. Soc. Am. B 25 (2008) A81.
[20] P. Bowlan, P. Gabolde, A. Schreenath, K. McGresham, S. Akturk, R. Trebino, Spatially Resolved Spectral Interferometry, Presented at Conference on Light and Electro Optics, Long Beach, California, 2006.
[21] P. Bowlan, P. Gabolde, A. Shreenath, K. McGresham, R. Trebino, Opt. Express 14 (2006) (1900) 11892.
[22] P. Bowlan, P. Gabolde, R. Trebino, Opt. Express 15 (2007) 10219.
[23] P. Bowlan, H. Valtna-Luknew, M. Lohmus, P. Piksarv, P. Saari, R. Trebino, Opt. Lett. 34 (2009) 2276.
[24] A.C. Kovaecs, K. Osvay, Zs Bor, Opt. Lett. 20 (1995) 788.
[25] A.P. Kovaecs, K. Osvay, G. Kurdi, M. Gorbe, J. Klenbniczki, Z. Bor, Appl. Phys. B 80 (2005) 165.
[26] K. Oba, P.-C. Sun, Y.T. Mazurenko, Y. Fainman, Appl. Opt. 38 (1999) 3810.
[27] R. Wyatt, E. Marinero, Appl. Phys. A: Mater. Sci. Process. 25 (1981) 297.
[28] P. Bowlan, R. Trebino, J. Opt. Soc. Am. B 27 (2010) 2322.
[29] A.S. Weling, D.H. Auston, J. Opt. Soc. Am. B 13 (1996) 2783.